Foam-Replicated Diopside/Fluorapatite/Wollastonite-Based Glass–Ceramic Scaffolds

ceramics

MDPI

Article

Foam-Replicated Diopside/Fluorapatite/Wollastonite-Based Glass–Ceramic Scaffolds

Francesco Baino [1,2,*], Dilshat U. Tulyaganov [3], Ziyodilla Kahharov [3], Abbas Rahdar [4] and Enrica Verné [1]

[1] Institute of Materials Physics and Engineering, Department of Applied Science and Technology, Politecnico di Torino, 10129 Turin, Italy; enrica.verne@polito.it
[2] Interdepartmental Center J-Tech, Politecnico di Torino, 10129 Turin, Italy
[3] Department of Natural-Mathematical Sciences, Turin Polytechnic University in Tashkent, Tashkent 100095, Uzbekistan; tulyaganovdilshat@gmail.com (D.U.T.); ziyod1811@gmail.com (Z.K.)
[4] Department of Physics, University of Zabol, Zabol 98613-35856, Iran; a.rahdarnanophysics@gmail.com
* Correspondence: francesco.baino@polito.it; Tel.: +39-011-090-4668

Abstract: Implantation of three-dimensional (3D) bioactive glass-derived porous scaffolds is an effective strategy for promoting bone repair and regeneration in large osseous defect sites. The present study intends to expand the potential of a SiO_2–P_2O_5–CaO–MgO–Na_2O–CaF_2 glass composition, which has already proven to be successful in regenerating bone in both animals and human patients. Specifically, this research work reports the fabrication of macroporous glass–ceramic scaffolds by the foam replica method, using the abovementioned bioactive glass powders as a parent material. The sinter-crystallization of the glass powder was investigated by hot-stage microscopy, differential thermal analysis, and X-ray diffraction. Scanning electron microscopy was used to investigate the pore–strut architecture of the resultant glass–ceramic scaffolds in which diopside, fluorapatite, and wollastonite crystallized during thermal treatment. Immersion studies in simulated body fluids revealed that the scaffolds have bioactive behavior in vitro; the mechanical properties were also potentially suitable to suggest use in load-bearing bone applications.

Keywords: bioactive glass; glass–ceramic; scaffold; porosity; bone tissue engineering

Citation: Baino, F.; Tulyaganov, D.U.; Kahharov, Z.; Rahdar, A.; Verné, E. Foam-Replicated Diopside/Fluorapatite/Wollastonite-Based Glass–Ceramic Scaffolds. *Ceramics* **2022**, *5*, 120–130. https://doi.org/10.3390/ceramics5010011

Academic Editors: Narottam P. Bansal, Ashutosh Goel and Gilbert Fantozzi

Received: 22 December 2021
Accepted: 18 February 2022
Published: 21 February 2022

1. Introduction

The continuous advancements in materials science and technology allow for developing more and more sophisticated products with special properties that are able to achieve specific applications and meet new needs. Biomaterials aim at replacing parts or restoring functions in the body that have been damaged or lost, in a safe, reliable, and naturally acceptable manner as well as at an affordable cost. As a general and similarity-based rule, an ideal biomaterial should display properties as close as possible to those of the tissues that it will replace [1].

Bioactive glasses and glass–ceramics are able to spontaneously convert their own surface into a hydroxyapatite layer in a biological environment. Research on this broad group of biomaterials began with the discovery of 45S5 glass composition (45SiO_2–24.5CaO–24.5Na_2O–6P_2O_5 wt %) by Larry Hench's team in the late 1960s [2]. Later, bioactive glasses and glass–ceramics in the form of porous scaffolds were found to be able to replicate—even to a great extent—the complex morphology of bone and promote the regeneration of natural tissue [3,4]. In this regard, 45S5 glass, which was considered the "gold standard" bone substitute for a long time, suffers from limited sintering ability that results in poorly densified porous glass–ceramics [5].

Bioactive glass scaffolds might be fabricated through various techniques including the foam replica method [6–8], sol–gel casting [9,10] freeze drying [11], robocasting [12,13], powder technologies originally developed in metallurgy [14,15], etc. A macroporous glass closely mimicking the morphology of the original sacrificial template can be produced

through the replica method, which involves the impregnation of a polymeric cellular structure with a glass suspension (slurry) or suitable precursor solution. Schwartzwalder and Somers [16] were the first to introduce this technique, encompassing (i) immersion of an open-cell element of spongy material in a slurry of a ceramic material, (ii) removal of excess slurry, and (iii) firing the impregnated polymer to get rid of the spongy material and form a hardened structure of porous ceramic. Since then, the foam replica technique has become the most popular way to fabricate macroporous ceramic, glass, and glass–ceramic products due to the high simplicity, effectiveness, inexpensiveness, and versatility of the method.

In 2006, the sponge replica technique was first implemented in bone tissue engineering for fabricating bioactive glass-derived scaffolds [6,17]. Polymer foam replication is a well-established technique to fabricate open-pore three-dimensional (3D) structures with a cell size in the range of 50 μm to 3 mm and total porosity of 40–95 vol % [18]. There are some important requirements that the organic foam should fulfill: the sponge characteristics have to be reproducible (i.e., narrow ranges of cell size and distribution are allowed) and the polymer should exhibit elastic behavior in order to restore its own shape after squeezing as well as be completely removable during sintering to avoid any contamination of the final product. Moreover, a thin glass coating should form on the struts of the original cellular structure when the excess suspension is removed. In order to coat the polymeric template efficiently, glass suspensions exhibiting shear-thinning behavior are required [19]. The other technological operations include drying of the glass-coated polymeric template, optionally followed by heat treatment between 300 °C and 800 °C at very low heating rates (around 1 °C/min) [20], and the final stage of sintering at an appropriate temperature depending on the material.

In this work, the sponge replica technique was applied to fabricate, for the first time, macroporous glass–ceramic scaffolds from a SiO_2–P_2O_5–CaO–MgO–Na_2O–CaF_2-based glass (called "1d") that demonstrated apatite-forming ability from the early stages of immersion in simulated body fluids and favored bone regeneration. In vitro cell cultures, in vivo animal tests, and early clinical trials showed excellent biocompatibility of 1d glass and low inflammatory response of the surrounding tissue [21,22]. Sintering of the corresponding glass powder compacts yielded glass–ceramics with mechanical properties matching those of dentine and jaw bone: flexural strength of 171 MPa, elastic modulus of 27 GPa, Vickers microhardness of 6.1 GPa, and fracture toughness of 1.7 MPa $m^{0.5}$ [23].

2. Materials and Methods

2.1. Materials

The reagents used for 1d glass preparation (high-purity powders of SiO_2 (purity > 99.5%), $CaCO_3$ (>99.5%), $MgCO_3$ (purity > 99.0%), Na_2CO_3 (>99.0%), $NH_4H_2PO_4$ (>99.0%) and CaF_2 (>99.9%)) were provided by Sigma-Aldrich (St. Louis, MO, USA). The salts and acid used for simulated body fluid (SBF) preparation were also provided by Sigma-Aldrich.

2.2. Preparation of Glass

The 1d glass used in this work as the parent material for making scaffolds was in a multicomponent 46.1SiO_2–28.7CaO–8.8MgO–6.2P_2O_5–5.7CaF_2–4.5Na_2O (wt %) compositional system. A batch of 100 g was prepared by weighing the reagents in the required proportion and thorough mixing/homogenization through ball-milling. The mix was preheated at 850 °C for 1 h in an Al_2O_3 crucible at a heating rate of 2.5 °C/min and then the glass was produced by melting the batch in a Pt crucible at 1420 °C for 1 h in air and by subsequent quenching of the melt in cold water (Figure 1a). After complete drying, glass frit was pulverized in a high-speed planetary mill (Figure 1b); the glass powder obtained was finally sifted through a stainless-steel sieve (mesh: 56 μm).

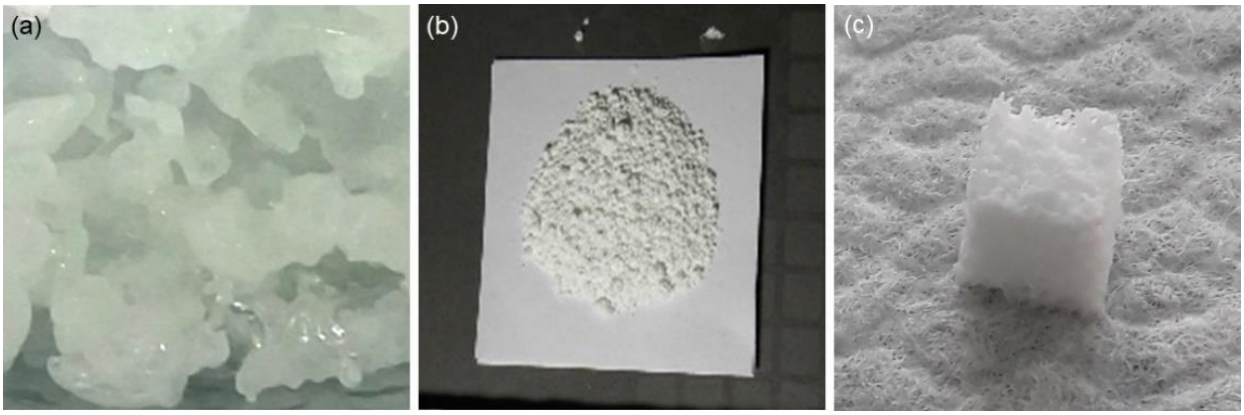

Figure 1. Visual appearance of the produced samples: (**a**) 1d glass frit, (**b**) glass powder after milling and (**c**) 1d glass-derived sintered scaffold (the size of scaffold is ~8 mm due to volumetric shrinkage taking place during sintering).

2.3. Fabrication of Scaffolds

Porous scaffolds based on 1d glass were produced by the foam replica method according to a processing schedule that was previously applied on a broad range of glass compositions [24]. Briefly, a polyurethane (PU) sponge panel (45 ppi) was cut into 10 mm × 10 mm × 10 mm cuboids using a scalpel, and the small foam blocks were then soaked in a glass-containing suspension to carry out the replication process. In order to prepare the glass slurry, poly(vinyl alcohol) was first dissolved in distilled water under continuous magnetic stirring (250 rpm, 80 °C); then the solution was cooled down to room temperature and a proper amount of glass powders was added to the batch (PVA:water:1d glass = 6:64:30, wt %). The slurry was stirred at room temperature for about 15 min at 250 rpm. The PU foam cuboids were dipped into the glass powder suspension three times; after each immersion, the sponge was placed onto a metallic grid and the excess slurry was squeezed out from the pores by applying a compression cycle during which the sponge thickness was sequentially reduced by 60% along the three spatial directions (50 kPa for about 1 s in each direction). Afterwards, sponges underwent a final stage of impregnation into the slurry without any further squeezing. Glass-coated polymeric foams were dried at room temperature for at least 6 h and thermally treated at 800 °C for 3 h in an electrically heated furnace (Nabertherm Muffle Furnace 1300 L9/11/SKM/P330, Lilienthal, Germany) at heating and cooling rates of 5 and 10 °C/min, respectively. An example of the resulting scaffold is shown in Figure 1c.

2.4. Characterizations

2.4.1. Thermal Analyses

The thermal behavior of 1d glass was studied by differential thermal analysis (DTA) and hot-stage microscopy (HSM) using a DTA 404 PC instrument (Netzsch, Selb, Germany) and a HSM EMI III equipment (Hesse Instruments, Osterode am Harz, Germany), respectively. In both analyses, the thermal range was 20 °C to 1000 °C and the heating rate was 5 °C/min (i.e., the heating rate used for scaffold production).

As regards DTA measurement, 100 mg of 1d glass powders were introduced in a small Pt–Rh crucible provided by the instrument manufacturer; an equal amount of high-purity (>99%) alumina powder was used as a reference material.

As regards HSM measurement, a small cylindrical sample of cold-pressed 1d glass powder (diameter = height = 3 mm) was positioned onto a high-purity alumina plate inside the furnace chamber. Black and white images showing the silhouettes of the sample were recorded during the thermal cycle and processed using dedicated software for image analysis (EMI III—Software für das Erhitzungsmikroskop, Hesse Instruments, Osterode am Harz, Germany), which quantified the decrease of normalized area (A/A_0) as a function

of temperature, where A_0 is the initial area of the cylinder silhouette at the beginning of the test (about 9 mm^2) and A is the area of the sample silhouette measured at increasing temperatures during the analysis.

2.4.2. Crystallization

Crystallization of 1d-derived scaffolds due to thermal treatment was studied by X-ray diffraction (XRD; X'Pert Pro PW3040/60 diffractometer, PANalytical, Eindhoven, The Netherlands). The analysis was performed using Bragg–Brentano camera geometry (Cu–Kα incident radiation, λ = 0.15405 nm) and varying the 2θ angle from 10 to 60°. The voltage and filament current were fixed at 40 kV and 30 mA, respectively. Data were acquired by fixing the step counting time at 1 s and the step size at 0.02°. The scaffold was pulverized prior to XRD investigations. Crystalline phases were identified by X'Pert HighScore software 2.2b (PANalytical) equipped with the PCPDFWIN database.

2.4.3. Morphology

The 1d-derived scaffolds were inspected by field-emission scanning electron microscopy (FE-SEM Supra^{TM} 40, Zeiss, Oberkochen, Germany) in order to assess the postsintering morphology and pore/strut sizes. The samples were sputter-coated with chromium before undergoing FE-SEM analysis and investigated at a voltage of 15 kV.

The total porosity (vol %) was calculated by density measurements as $(1 - \rho/\rho_0) \times 100$, where ρ is the apparent density of the scaffold (mass-to-volume ratio) and ρ_0 is the bulk density. Pore size distribution was assessed by microcomputed tomography (micro-CT) using custom-made equipment available at J-Tech Center.

2.4.4. Mechanical Properties

The samples underwent crushing tests using a Model 43 MTS machine (MTS, Eden Prairie, MN, USA) with a cell load of 5 kN and a cross-head speed of 1 mm/min. The compressive strength (MPa) was calculated as the ratio between the maximum load observed during the test and the resistant cross-sectional area, which was measured for each sample using digital calipers.

The elastic modulus was estimated from the initial linear region of the stress–strain curve.

The mechanical results were expressed as the mean ± standard deviation, assessed on five specimens.

2.4.5. In Vitro Bioactivity

The apatite-forming ability of scaffolds was assessed by immersion studies in SBF, which was prepared according to the protocol reported by Kokubo and Takadama [25]. A mass-to-volume ratio of 1.5 mg/mL was used, as suggested in a previous study by the Technical Committee 4 (TC04) of the International Commission on Glass (ICG) [26]. During the experiments, the scaffolds were stored in sealed plastic bottles placed inside a static incubator at 37 °C. The solution in each bottle was fully replaced with new SBF every 48 h in order to simulate fluid circulation in physiological conditions and the pH was monitored daily using a digital pH-meter. At each time point (48 h, one week, and two weeks), the samples were removed from the container, gently washed with distilled water, left to dry overnight in a hood, and finally stored in a sealed plastic box before undergoing morphological and compositional investigation (FE-SEM equipped with energy-dispersive spectroscopy (EDS)).

3. Results and Discussion

The characteristic temperatures T_g (glass transition), T_x (onset of crystallization), and T_p (peak of crystallization) of 1d glass were assessed from the DTA plot and found to be 640 °C, 785 °C, and 830 °C, respectively (Figure 2). The HSM curve plotted in Figure 2 reveals that 1d glass has a one-step densification behavior with maximum area reduction A/A_0 = 0.70, which is consistent with the value determined by Kansal et al. [27] for the

same material ($A/A_0 = 0.69$). Specifically, densification began at $T_{FS} \approx T_g$ (first shrinkage, onset of viscous flow sintering) and continued until the maximum shrinkage was reached (T_{MS} = 770 °C). The sintering temperature for producing the scaffolds (800 °C) was chosen in the plateau following the maximum densification, with the middle value in the range of T_{MS} to T_P.

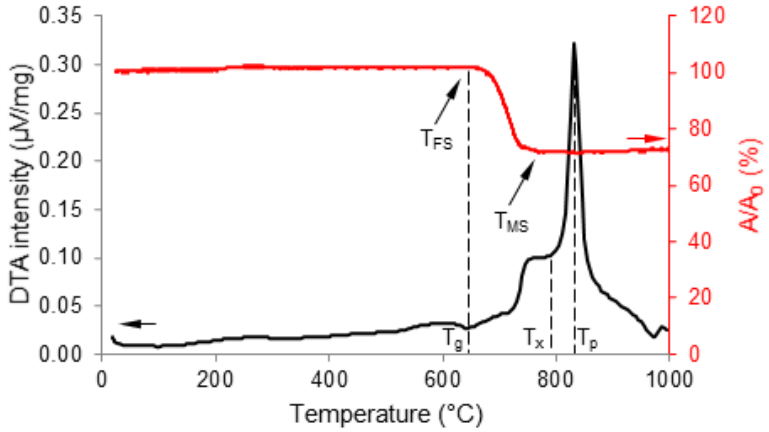

Figure 2. Thermal analyses of 1d glass: DTA and HSM.

The XRD pattern shown in Figure 3a exhibits the typical broad halo (also called an "amorphous halo") of silicate glasses (2θ range of 25 to 38°) without any diffraction peaks, thus confirming that the as-quenched material is actually in the glassy state. The thermal treatment at 800 °C, which was applied to sinter glass particles and allows scaffold consolidation, also promoted devitrification of the material (Figure 3b). Specifically, three crystalline phases were detected, i.e., $CaMgSi_2O_6$ (diopside, ICDD card 01-071-1067), fluorapatite ($Ca_{10}(PO_4)_6F_2$, ICDD card 01-071-880), and wollastonite ($CaSiO_3$, ICDD card 01-042-0550). These results are consistent with previous findings on the crystallization of 1d glass around 800 °C [28]. All three crystalline phases are highly biocompatible and suitable for being applied in bone repair surgery as fluorapatite occurs naturally in the mixed bio-apatites that form the mineral phase of bones and teeth in mammals [29]; wollastonite has been well known as an osseous substitute since the 1980s, when Kokubo's team developed the first machinable apatite/wollastonite bioactive glass–ceramics [30]; and diopside was more recently claimed to be superior to other silicate bioceramics due to its better mechanical properties, slower dissolution rate, improved apatite-forming ability, and excellent in vivo biocompatibility [31].

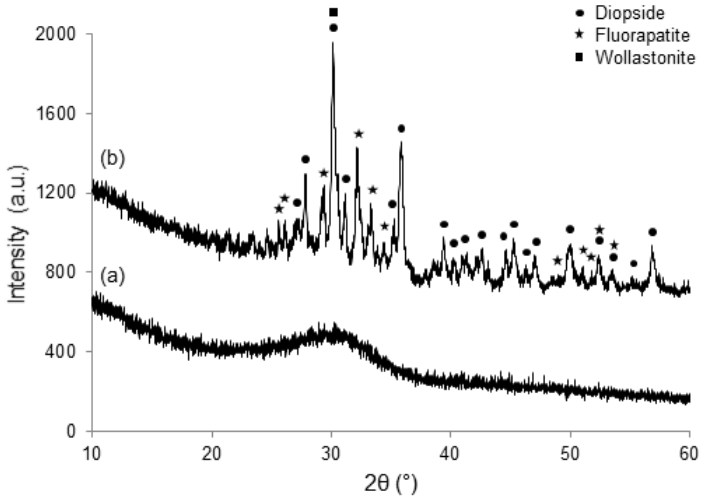

Figure 3. XRD plot of (**a**) 1d glass and (**b**) 1d glass-derived scaffolds (ground into a powder) produced by sintering at 800 °C for 3 h.

The multiphase glass–ceramic material obtained by sinter–crystallization of 1d glass has the benefit of synergistically combining the regenerative effects of the different phases; this aspect deserves further research. The properties and biomedical applications of the single crystalline phases are discussed elsewhere in detail. Ressler et al. [32] comprehensively reviewed ion-substituted hydroxyapatites—including fluorapatite—and Pajor et al. [33] highlighted the importance of F-doped apatite for dental regenerative applications because of its lower solubility in an acidic environment (like the mouth) as compared to pure hydroxyapatite. Calcium silicate bioceramics were also reviewed in a recent paper [34]. Both calcium phosphates and calcium silicates were used to fabricate porous ceramic scaffolds for tissue engineering [35]; it was also suggested that porous β-wollastonite has better bone regenerative potential compared to β-tricalcium phosphate scaffolds when implanted in vivo (rabbit calvarial defect model) [36].

Figure 4a,b shows some details of the 3D glass–ceramic replica of the polymeric foam that was obtained after polymer burnoff and glass powder sinter–crystallization. FE-SEM analysis displays the presence of a 3D network of interconnected macropores (estimated size: above 100 μm) that closely mimics the pore–strut architecture of trabecular bone. These are key features for implantable bone tissue engineering scaffolds in order to have paths for living cells to migrate, new tissue to grow in, nutrients to enter the pores, and metabolic waste products to flow out. The pore size distribution, displayed in Figure 5, reveals that most pore volume (about 60%) is attributable to pores larger than 300 μm, which are expected to promote direct osteogenesis in vivo due to vascularization and high oxygenation [37]. The surfaces of scaffold struts, displayed in Figure 4c, exhibit a certain roughness created by small surface pores (pit size of around 1 μm or below); this can be an inherent added value from a biological point of view because osteoblast adhesion is promoted onto micro-rough and nano-rough biomedical surfaces as compared to relatively smooth implant materials [38].

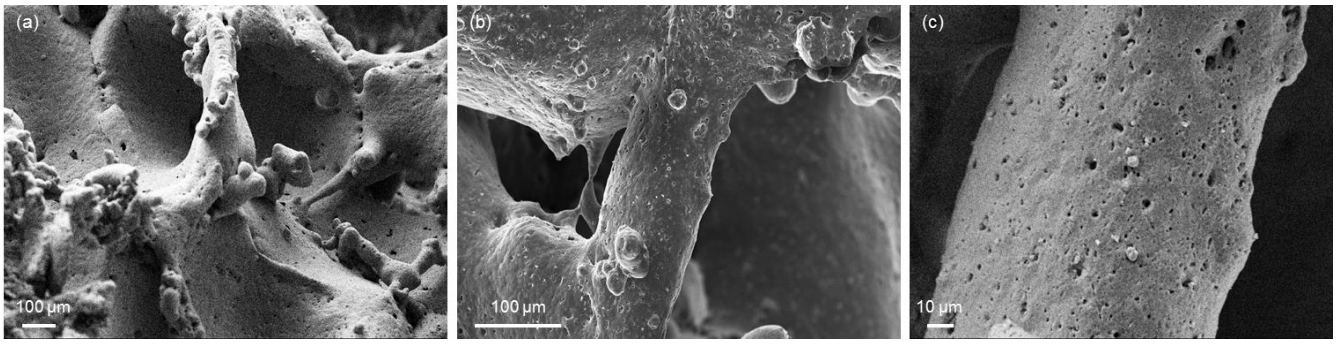

Figure 4. Investigation of 1d-derived scaffold morphology: (**a**) 3D pore–strut architecture, (**b**) sintered strut, and (**c**) details of the surface of the strut.

The total porosity of 1d-derived scaffolds (68 ± 10 vol %) is comparable to that of human healthy cancellous bone (50–80 vol % [39,40]) and falls into the optimal range recommended for tissue engineering scaffolds [41].

An example of stress–strain curve (compressive test) for 1d-derived scaffolds is reported in Figure 6. The curve has a multipeak profile, which is typical of ceramic foams [42]. The curve has an initial positive slope up to a first series of peaks, after which the thin trabeculae begin to crack, causing an apparent stress drop (negative slope). However, the scaffold was still able to withstand higher loads and, therefore, the stress repeatedly rose, yielding a jagged curve profile (in the intermediate region of the plot), associated with the progressive cracking of scaffold struts. When the thicker struts also cracked, the curve exhibited a final negative slope before reaching complete fracture of the scaffold.

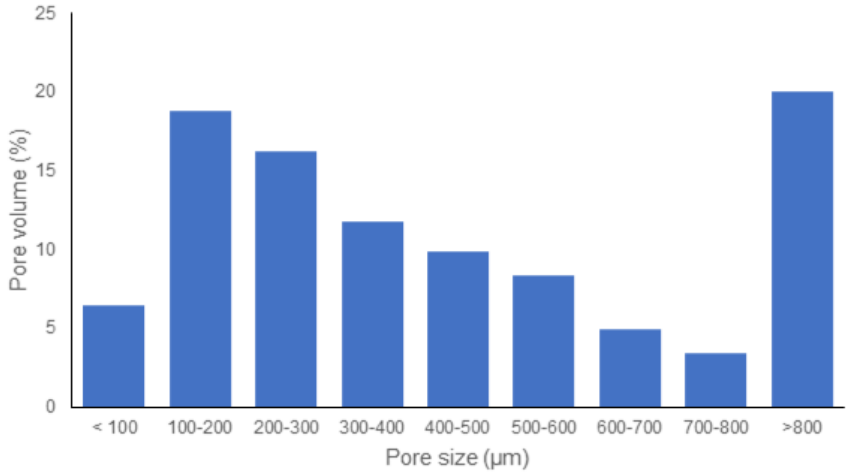

Figure 5. Pore size distribution in 1d-derived scaffolds assessed by micro-CT measurement.

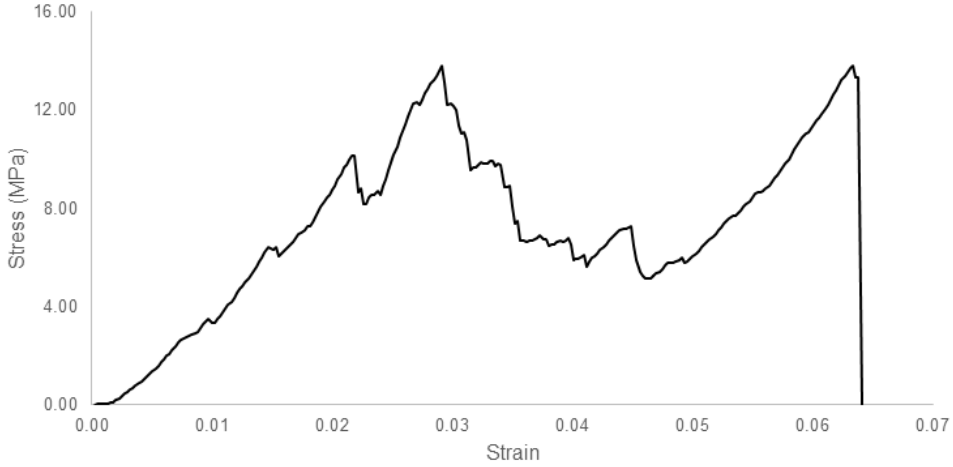

Figure 6. Typical stress–strain curve (compressive test) of 1d-derived scaffolds.

The compressive strength of scaffolds is 29.7 ± 14.9 MPa, which is well above the standard reference range considered for human trabecular bone (2–12 MPa [2]) and suggests potential suitability for implantation in load-bearing sites, too.

The elastic modulus of scaffolds determined from the stress–strain curve is 1.4 ± 0.4 GPa, which can be considered acceptable for applications in contact with bone tissue, although the reference data are quite variable. For example, Thompson and Hench [43] reported the elastic modulus of human spongy bone in the range of 50 to 500 MPa, while Keaveny [44] had significantly higher values (1–4 GPa).

Gibson and Ashby [45] demonstrated that the elastic modulus (E) of low-density ceramic foams, like the scaffolds studied in the present work, is primarily dictated by the total porosity (p) according to a simple second-order power law, as follows:

$$E = E_0(1 - p)^2 \quad (1)$$

where E_0 is the elastic modulus of the bulk (nonporous) material.

The mechanical properties of 1d-derived glass–ceramics, produced by sinter–crystallization of glass powder compacts, were determined by Dimitriadis et al. [46], who reported elastic moduli of 11.0 and 26.6 GPa for samples undergoing thermal treatment at 750 °C and 850 °C, respectively. Substituting these values of E_0 (along with p = 0.68) into Equation (1), we obtain E_1 = 1.12 GPa and E_2 = 2.72 GPa. Therefore, our experimental results are in good accordance with the theoretical estimations as the elastic modulus of the scaffolds sintered at 800 °C fell in the range of E_1 to E_2.

Results from in vitro bioactivity tests in SBF (Figure 7) showed that 1d-derived scaffolds have good apatite-forming ability, regardless of the presence of crystalline phases, which usually decrease the rate of bioactivity kinetics in many bioactive glass systems, like 45S5 Bioglass® [47]. The general reactions yielding the formation of calcium phosphate/hydroxyapatite on the surface of bioactive glasses upon immersion in SBF have been described elsewhere in detail [2] and can also be applied to the present case. After immersion for just 48 h, the surface of scaffold struts appeared to be covered by a thin layer of a newly-formed phase composed of small spherical agglomerates (Figure 7a–c). A compositional analysis revealed that the new phase was a calcium phosphate layer with Ca-to-P atomic ratio equal to 1.78. The cracks on the surface of this newly-formed phase (Figure 7c) are associated with the presence of a silica gel layer lying underneath the calcium phosphate phase, as described by the bioactivity mechanism proposed by Hench's research team [48]; the silica gel layer tends to crack due to the drying of the samples and the high vacuum applied in the chamber of SEM equipment. Small globular agglomerates were also observed on the inner surface of the pores, suggesting that the SBF could permeate the whole volume of the scaffold due to the interconnected porous architecture achievable through using foam replication as the scaffold manufacturing method. Despite the formation of this surface layer, the scaffold macropores remained open and interconnected, and the overall 3D macro-architecture was not significantly altered (Figure 7a,d,g). The thickness of the calcium phosphate layer increased over time (Figure 7e,h), qualitatively confirming the continuous ion exchange between the glass–ceramic material and SBF, as well as the progress of in vitro bioactivity mechanism. After one week in SBF, compositional analysis revealed that the intensity of the peak of Si (typical of the 1d-derived glass–ceramic material and silica-gel reaction layer) significantly decreased, while the intensities of the peaks of Ca and P increased (results not shown), thus further confirming the growth of a surface calcium phosphate layer that covers the scaffold struts lying underneath. The typical globular morphology of this calcium phosphate layer (Figure 7f,i) is the "fingerprint" of the biomineralization process taking place on bioactive glasses immersed in biological fluids. After one week, the Ca-to-P atomic ratio decreased to 1.50, which suggests the formation of Ca-deficient hydroxyapatite on the scaffold surface, in agreement with the results reported in other studies on several bioactive silicate glass and glass–ceramic compositions [49–51]. After two weeks, the cracks on the hydroxyapatite layer are no longer visible and a homogenous and continuous "biomimetic skin" completely covers the scaffold surface and struts (Figure 7h,i). This observation is also supported by compositional analysis (results not shown), as the peak of Si in the EDS spectrum was hardly visible and the Ca-to-P atomic ratio increased to 1.60, approaching the stoichiometric value (1.67) for hydroxyapatite. These results are consistent with those reported by Dimitriadis et al. [46], who assessed the presence of hydroxyapatite on 1d-derived compact samples undergoing sinter–crystallization at 850 °C and subsequent immersion in SBF.

Formation of a hydroxyapatite layer on the surface of biomaterials is commonly considered a key requirement to allow interfacial bonding with living bone after implantation in the human body as bone cells (especially osteoblasts) preferably attach and proliferate on such a nanostructured calcium phosphate layer, thus producing new bone [52]. The 1d material in the glassy state was already proven to be able to bond to bone and stimulate new alveolar bone formation in human patients in a small clinical study [22]; therefore, the results reported in the current study are highly promising to support the suitability of glass–ceramic scaffolds based on 1d glass for use in bone/dental applications.

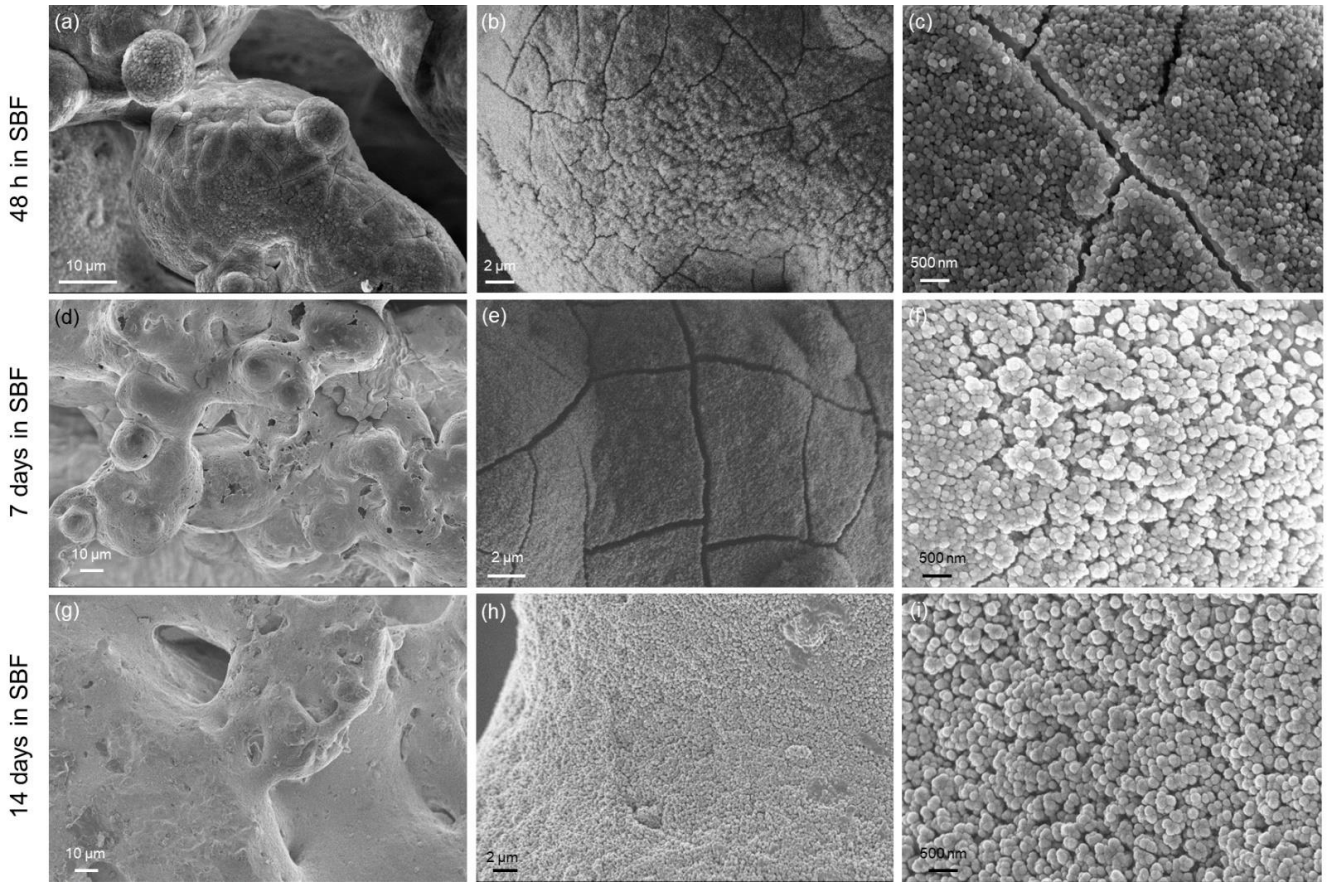

Figure 7. In vitro bioactivity tests: surface of scaffold struts at increasing magnifications after immersion in SBF for (**a**–**c**) 48 h, (**d**–**f**) 1 week, and (**g**–**i**) 2 weeks.

4. Conclusions

Porous glass–ceramic scaffolds were produced by foam replication using a SiO_2–P_2O_5–CaO–MgO–Na_2O–CaF_2 glass with proved bone-regenerative properties as a starting material. Upon high-temperature thermal treatment, the glass underwent sinter–crystallization, leading to consolidation of the scaffold structure and concurrent development of three biocompatible crystalline phases, i.e., diopside, fluorapatite, and wollastonite. The scaffolds exhibited a 3D pore–strut architecture and total porosity (68 vol %) matching those of spongy bone, while the compressive strength (29.7 MPa) and elastic modulus (1.4 GPa) were superior to those of osseous tissue, suggesting suitability for application in load-bearing sites. The scaffolds also exhibited highly promising bioactive properties in vitro, being covered by a calcium phosphate layer after immersion in simulated body fluids for just 48 h.

Author Contributions: Conceptualization, F.B. and D.U.T.; methodology, F.B., D.U.T., Z.K., A.R. and E.V.; investigation, F.B., D.U.T., Z.K., A.R. and E.V.; writing—original draft preparation, F.B. and D.U.T.; writing—review and editing, F.B., D.U.T., Z.K., A.R. and E.V. All authors have read and agreed to the published version of the manuscript.

Funding: This research received no external funding.

Institutional Review Board Statement: Not applicable.

Informed Consent Statement: Not applicable.

Data Availability Statement: Data available in the paper.

Conflicts of Interest: The authors declare no conflict of interest.

References

1. Baino, F.; Ferraris, M. Learning from Nature: Using bioinspired approaches and natural materials to make porous bioceramics. *Int. J. Appl. Ceram. Technol.* **2017**, *14*, 507–520. [CrossRef]
2. Hench, L.L. Bioceramics—From concept to clinic. *J. Am. Ceram. Soc.* **1991**, *74*, 1487–1510. [CrossRef]
3. Boccardi, E.; Philippart, A.; Juhasz-Bortuzzo, J.A.; Novajra, G.; Vitale-Brovarone, C.; Boccaccini, A.R. Characterisation of Bioglass based foams developed via replication of natural marine sponges. *Adv. Appl. Ceram.* **2015**, *114* (Suppl. 1), S56–S62. [CrossRef]
4. Falvo D'Urso Labate, G.; Catapano, G.; Vitale-Brovarone, C.; Baino, F. Quantifying the micro-architectural similarity of bioceramic scaffolds to bone. *Ceram. Int.* **2017**, *43*, 9443–9450. [CrossRef]
5. Baino, F.; Ferraris, M.; Bretcanu, O.; Verné, E.; Vitale-Brovarone, C. Optimization of composition, structure and mechanical strength of bioactive 3-D glass-ceramic scaffolds for bone substitution. *J. Biomater. Appl.* **2013**, *27*, 872–890. [CrossRef]
6. Chen, Q.Z.; Thompson, I.D.; Boccaccini, A.R. 45S5 Bioglass derived glass ceramic scaffolds for bone tissue engineering. *Biomaterials* **2006**, *27*, 2414–2425. [CrossRef]
7. Chen, Q.; Mohn, D.; Stark, W.J. Optimization of Bioglass® scaffold fabrication process. *J. Am. Ceram. Soc.* **2011**, *94*, 4184–4190. [CrossRef]
8. Studart, A.; Gonzenbach, U.T.; Tervoort, E.; Gauckler, L.J. Processing routes to macroporous ceramics: A review. *J. Am. Ceram. Soc.* **2006**, *89*, 1771–1789. [CrossRef]
9. Rezwan, K.; Chen, Q.Z.; Blaker, J.J.; Boccaccini, A.R. Biodegradable and bioactive porous polymer/inorganic composite scaffolds for bone tissue engineering. *Biomaterials* **2006**, *27*, 3413–3431. [CrossRef]
10. Jones, J.; Hench, L.L. Regeneration of trabecular bone using porous ceramics. *Curr. Opin. Solid State Mater. Sci.* **2003**, *7*, 301–307. [CrossRef]
11. Fukasawa, T.; Deng, Z.Y.; Ando, M.; Ohji, T.; Goto, Y. Pore structure of porous ceramics synthesized from water-based slurry by freeze-dry process. *J. Mater. Sci.* **2001**, *36*, 2523–2527. [CrossRef]
12. Leong, K.F.; Cheah, C.M.; Chua, C.K. Solid freeform fabrication of three-dimensional scaffolds for engineering replacement tissues and organs. *Biomaterials* **2003**, *24*, 2363–2378. [CrossRef]
13. Barberi, J.; Baino, F.; Fiume, E.; Orlygsson, G.; Nommeots-Nomm, A.; Massera, J.; Verné, E. Robocasting of SiO_2-based bioactive glass scaffolds with porosity gradient for bone regeneration and potential load-bearing applications. *Materials* **2019**, *12*, 2691. [CrossRef] [PubMed]
14. Aguilar-Reyes, E.A.; Leon-Patino, C.A.; Jacinto-Diaz, B.; Lefebvre, L.P. Structural characterization and mechanical evaluation of bioactive glass 45S5 foams obtained by a powder technology approach. *J. Am. Ceram. Soc.* **2012**, *95*, 3776–3780. [CrossRef]
15. Aguilar-Reyes, E.A.; Leon-Patino, C.A.; Jacinto-Diaz, B.; Lefebvre, L.P. Synthesis of 45S5 Bioglass® foams by a powder metallurgy approach. *Mater. Sci. Technol.* **2010**, *17*, 70–77.
16. Schwartzwalder, K.; Somers, A.V. Method of Making Porous Ceramic Articles. U.S. Patent 3,090,094, 21 May 1963.
17. Park, Y.S.; Kim, K.N.; Kim, K.M.; Choi, S.H.; Kim, C.K.; Legeros, R.Z.; Lee, Y.K. Feasibility of three-dimensional macroporous scaffold using calcium phosphate glass and polyurethane sponge. *J. Mater. Sci.* **2006**, *41*, 4357–4364. [CrossRef]
18. Fiume, E.; Ciavattini, S.; Verné, E.; Baino, F. Foam replica method in the manufacturing of bioactiveglassscaffolds: Out-of-date technology or still underexploited potential? *Materials* **2021**, *14*, 2795. [CrossRef]
19. Alonso, S.; Palomo, A. Alkaline activation of metakaolin and calcium hydroxide mixtures: Influence of temperature, activator concentration and solids ratio. *Mater. Lett.* **2001**, *47*, 55–62. [CrossRef]
20. Duxson, P.; Lukey, G.C.; Separovic, F.; Van Deventer, J.S.J. Effect of alkali cations on aluminum incorporation in geopolymeric gels. *Ind. Eng. Chem. Res.* **2005**, *44*, 832839. [CrossRef]
21. Schmitz, S.I.; Widholz, B.; Essers, C.; Becker, M.; Tulyaganov, D.U.; Moghaddama, A.; Gonzalo de Juan, I.; Westhauser, F. Superior biocompatibility and comparable osteoinductive properties: Sodium-reduced fluoride-containing bioactive glass belonging to the CaO–MgO–SiO_2 system as a promising alternative to 45S5 bioactive glass. *Bioactive Mater.* **2020**, *5*, 55–65. [CrossRef]
22. Tulyaganov, D.U.; Makhkamov, M.E.; Urazbaev, A.; Goel, A.; Ferreira, J.M.F. Synthesis, processing and characterization of a bioactive glass composition for bone regeneration. *Ceram. Int.* **2013**, *39*, 2519–2526. [CrossRef]
23. Dimitriadis, K. Development of Glass-Ceramics for Dental Applications. Ph.D. Thesis, University of Ioannina, Ioannina, Greece, 2020.
24. Fiume, E.; Serino, G.; Bignardi, C.; Verné, E.; Baino, F. Sintering behavior of a six-oxide silicate bioactive glass for scaffold manufacturing. *Appl. Sci.* **2020**, *10*, 8279. [CrossRef]
25. Kokubo, T.; Takadama, H. How useful is SBF in predicting in vivo bone bioactivity? *Biomaterials* **2006**, *27*, 2907–2915. [CrossRef] [PubMed]
26. Maçon, A.L.B.; Kim, T.B.; Valliant, E.M.; Goetschius, K.; Brow, R.K.; Day, D.E.; Hoppe, A.; Boccaccini, A.R.; Kim, I.Y.; Ohtsuki, C.; et al. A unified in vitro evaluation for apatite-forming ability of bioactive glasses and their variants. *J. Mater. Sci. Mater. Med.* **2015**, *26*, 115. [CrossRef] [PubMed]
27. Kansal, I.; Tulyaganov, D.U.; Goel, A.; Pascual, M.J.; Ferreira, J.M.F. Structural analysis and thermal behaviour of diopside-fluorapatite–wollastonite-based glasses and glass-ceramics. *Acta Biomater.* **2010**, *6*, 4380–4388. [CrossRef] [PubMed]
28. Tulyaganov, D.U.; Agathopoulos, S.; Valerio, P.; Balamurugan, A.; Saranti, A.; Karakassides, M.A.; Ferreira, J.M.F. Synthesis, bioactivity and preliminary biocompatibility studies of glasses in the system CaO–MgO–SiO_2–Na_2O–P_2O_5–CaF_2. *J. Mater. Sci. Mater. Med.* **2011**, *22*, 217–227. [CrossRef]
29. Boskey, A.L. Mineralization of bones and teeth. *Elements* **2007**, *6*, 385–392. [CrossRef]

30. Kokubo, T.; Ito, S.; Sakka, S.; Yamamuro, T. Formation of a highstrength bioactive glass-ceramic in the system MgO-CaO-SiO_2-P_2O_5. *J. Mater. Sci.* **1986**, *21*, 536–540. [CrossRef]
31. Wu, C.; Chang, J. Degradation, bioactivity, and cytocompatibility of diopside, akermanite, and bredigite ceramics. *J. Biomed. Mater. Res. B* **2007**, *83*, 153–160. [CrossRef]
32. Ressler, S.A.; Zuzic, A.; Ivanisevic, I.; Kamboj, N.; Ivankovic, H. Ionic substituted hydroxyapatite for bone regeneration applications: A review. *Open Ceram.* **2021**, *6*, 100122. [CrossRef]
33. Pajor, K.; Pajchel, L.; Kolmas, J. Hydroxyapatite and fluorapatite in conservative dentistry and oral implantology—A review. *Materials* **2019**, *12*, 2683. [CrossRef] [PubMed]
34. Kumar Venkatraman, S.; Swamiappan, S. Review on calcium- and magnesium-based silicates for bone tissue engineering applications. *J. Biomed. Mater. Res. A* **2020**, *108*, 1546–1562. [CrossRef] [PubMed]
35. Kamboj, N.; Ressler, A.; Hussainov, I. Bioactive ceramic scaffolds for bone tissue engineering by powder bed selective laser processing: A review. *Materials* **2021**, *14*, 5338. [CrossRef] [PubMed]
36. Xu, S.; Lin, K.; Wang, Z.; Chang, J.; Wang, L.; Lu, J.; Ning, C. Reconstruction of calvarial defect of rabbits using porous calcium silicate bioactive ceramics. *Biomaterials* **2008**, *29*, 2588–2596. [CrossRef]
37. Karageorgiou, V.; Kaplan, D. Porosity of 3D biomaterial scaffolds and osteogenesis. *Biomaterials* **2005**, *26*, 5474–5491. [CrossRef]
38. Spriano, S.; Yamaguchi, S.; Baino, F.; Ferraris, S. A critical review of multifunctional titanium surfaces: New frontiers for improving osseointegration and host response, avoiding bacteria contamination. *Acta Biomater.* **2018**, *79*, 1–22. [CrossRef]
39. Hildebrand, T.; Laib, A.; Muller, R.; Dequeker, J.; Ruegsegger, P. Direct three-dimensional morphometric analysis of human cancellous bone: Microstructural data from spine, femur, iliac crest, and calcaneus. *J. Bone Miner. Res.* **1999**, *14*, 1167–1174. [CrossRef]
40. Kim, J.; Shin, J.; Oh, S.; Yi, W.; Heo, M.; Lee, S.; Choi, S.; Huh, K. The three-dimensional microstructure of trabecular bone: Analysis of site-specific variation in the human jaw bone. *Imaging Sci. Dent.* **2013**, *43*, 227–233. [CrossRef]
41. Baino, F.; Fiume, E.; Barberi, J.; Kargozar, S.; Marchi, J.; Massera, J.; Verné, E. Processing methods for making porous bioactive glass-based scaffolds—A state-of-the-art review. *Int. J. Appl. Ceram. Technol.* **2019**, *16*, 1762–1796. [CrossRef]
42. Rice, R. Mechanical properties. In *Cellular Ceramics: Structure, Manufacturing, Properties and Applications*; Schaufer, M., Colombo, P., Eds.; Wiley: New York, NY, USA, 2005; pp. 291–312.
43. Thompson, I.D.; Hench, L.L. Mechanical properties of bioactive glasses, glass-ceramics and composites. *Proc. Inst. Mech. Eng. Part H J. Eng. Med.* **1998**, *212*, 127–136. [CrossRef]
44. Keaveny, T.M. Mechanistic approaches to analysis of trabecular bone. *Forma* **1997**, *12*, 267–275.
45. Gibson, L.J.; Ashby, F. The mechanics of three-dimensional cellular materials. *Proc. R. Soc. Lond. A* **1982**, *382*, 43–59.
46. Dimitriadis, K.; Moschovas, D.; Tulyaganov, D.U.; Agathopoulos, S. Development of novel bioactive glass-ceramics in the Na_2O/K_2O-CaO-$MgOSiO_2$-P_2O_5-CaF_2 system. *J. Non-Cryst. Solids* **2020**, *533*, 119936. [CrossRef]
47. Clupper, D.C.; Hench, L.L. Crystallization kinetics of tape cast bioactive glass 45S5. *J. Non-Cryst. Solids* **2003**, *318*, 43–48. [CrossRef]
48. Pantano, C.G.; Clark, A.E.; Hench, L.L. Multilayer corrosion films on Bioglass surfaces. *J. Am. Ceram. Soc.* **1974**, *57*, 412–413. [CrossRef]
49. López-Noriega, A.; Arcos, D.; Izquierdo-Barba, I.; Sakamoto, Y.; Terasaki, O.; Vallet-Regi, M. Ordered mesoporous bioactive glasses for bone tissue regeneration. *Chem. Mater.* **2006**, *18*, 3137–3144. [CrossRef]
50. Baino, F.; Fiume, E.; Miola, M.; Leone, F.; Onida, B.; Verné, E. Fe-doped bioactive glass-derived scaffolds produced by sol-gel foaming. *Mater. Lett.* **2019**, *235*, 207–211. [CrossRef]
51. Fiume, E.; Serino, G.; Bignardi, C.; Verné, E.; Baino, F. Bread-derived bioactive porous scaffolds: An innovative and sustainable approach to bone tissue engineering. *Molecules* **2019**, *24*, 2954. [CrossRef]
52. Mozafari, M.; Banijamali, S.; Baino, F.; Kargozar, S.; Hill, R.G. Calcium carbonate: Adored and ignored in bioactivity assessment. *Acta Biomater.* **2019**, *91*, 35–47. [CrossRef]